Removal of Rhodamine B from Aqueous Solution Using Palm Shell-Based Activated Carbon: Adsorption and Kinetic Studies

Maedeh Mohammadi,[†,‡] Ali J. Hassani,[†] Abdul Rahman Mohamed,[*,†] and Ghasem D. Najafpour[‡]

School of Chemical Engineering, Engineering Campus, Universiti Sains Malaysia, 14300 Nibong Tebal, Penang, Malaysia, and Faculty of Chemical Engineering, Noushirvani University of Technology, Babol, Iran

Palm shell derived activated carbon was utilized as a potential adsorbent to remove rhodamine B (RB) from aqueous solution. Activated carbon was prepared from palm shell through a physiochemical activation process to yield a sample with a Brunauer−Emmett−Teller (BET) surface area of 476.8 $m^2 \cdot g^{-1}$. The ability of the prepared activated carbon for dye adsorption was examined in a series of batch experiments. The effect of various process parameters such as initial dye concentration [(41.8 to 208.8) $\mu mol \cdot L^{-1}$], solution pH (3 to 11), and temperature [(30 to 50) °C] on the adsorption capacity of the adsorbent was investigated. Various adsorption isotherms (Langmuir, Freundlich, and Temkin) were used to interpret the experimental data. The obtained sorption data were reasonably described by the Langmuir model. The Temkin isotherm confirmed the presence of a repulsive lateral interaction in the adsorbent surface. Pseudofirst- and second-order kinetic models were used to predict the kinetics of the adsorption process. The obtained results revealed that the adsorption of RB on activated carbon followed a pseudosecond-order kinetic model. A maximum dye removal efficiency of 95 % was achieved at an initial dye concentration of 62.6 $\mu mol \cdot L^{-1}$, pH of 3, and temperature of 50 °C.

Introduction

Dyes and pigments are widely used in various industries to color the final product. They are applied in chemical laboratories for analytical purposes and also in many biomedical and biological laboratories as biological stain.[1] Rhodamine B (RB) is one of the most important dyes within the category of dyestuffs, which has been extensively used as a colorant in the textile and food industries and also as a biological stain in biomedical laboratories.[2,3] Currently, the use of this compound in foods and cosmetics is banned[4] as it contains four *N*-ethyl groups at either side of a xanthene ring which makes it toxic and carcinogenic. The treatment of effluents containing such compounds is of utmost importance due to the environmental impact created by such wastewaters.

Several approaches have been found in the literature dealing with the removal of RB from industrial and biological effluents. Photocatalytic degradation,[5−12] ultrasonic decomposition,[3,13] sonochemical degradation,[14,15] microbiological decomposition,[16−19] ion flotation,[1] liquid−liquid extraction through membrane technology,[2,20] and adsorption on various inorganic or organic matrices are some of the applied techniques in this area. A survey of the literature revealed that most research conducted in this field refers to photocatalytic degradation, and little attention has been paid to the adsorption technique. Although adsorption may appear to be a costly method, the use of low cost materials as adsorbent makes the adsorption process cost-effective.[21]

* Corresponding author. Tel.: +60 4 599 6410; fax: +60 4 594 1013. E-mail address: chrahman@eng.usm.my (A. R. Mohamed).
[†] Universiti Sains Malaysia. E-mail: mohammadi_fanni@yahoo.com (M.M.) and ahj_ir@yahoo.com (A.J.H.).
[‡] Noushirvani University of Technology. E-mail: najafpour@nit.ac.ir (G.D.N.).

Activated carbons have shown great potential for dye removal due to properties such as large surface area, microporous structure, and high adsorption capacity.[22] The high cost of activated carbon promotes the search for cheap materials mainly derived from biological origin. It has been proved that lignocellulosic biomasses are attractive resources for the preparation of carbonaceous materials implemented in adsorption processes.[21] The eco-friendly nature of lignocellulosic biomasses, their availability, and low cost are the main advantages of these resources, which makes them a suitable precursor for activated carbon preparation.[22] Various lignocellulosic biomasses such as Jute stick,[23] coconut coir pith,[24] Bagasse pith,[25] sawdust, and sugar cane[22] have been used naturally or in the form of activated carbon to remove RB from the aqueous phase through the adsorption process.

Palm shell is a waste material originating in significant amounts from the palm oil industry. Malaysia is the largest producer and exporter of palm oil in the world. Annually, 4.6 million tons of palm shell is generated as the byproduct of the palm industry in Malaysia.[26,27] Although part of the generated palm shell is utilized as fuel to generate process steam in palm processing mills, large quantities still have no specific use.[26,28] They are burnt in the open air or dumped which generates black smoke and serious environmental problems.

The large amount of palm shell generated in Malaysia can be utilized as a potential carbonaceous source for the preparation of activated carbon for adsorption applications. The present study aims to investigate the removal of RB from aqueous solution using palm shell derived activated carbon. The fabricated activated carbon was characterized in terms of microporosity and surface area, and then it was used to remove RB from aqueous solution. The effect of various operational parameters (dye concentration, solution pH, and temperature) on dye removal efficiency was examined. Also, several adsorp-

10.1021/je100730a
Published on Web 11/08/2010

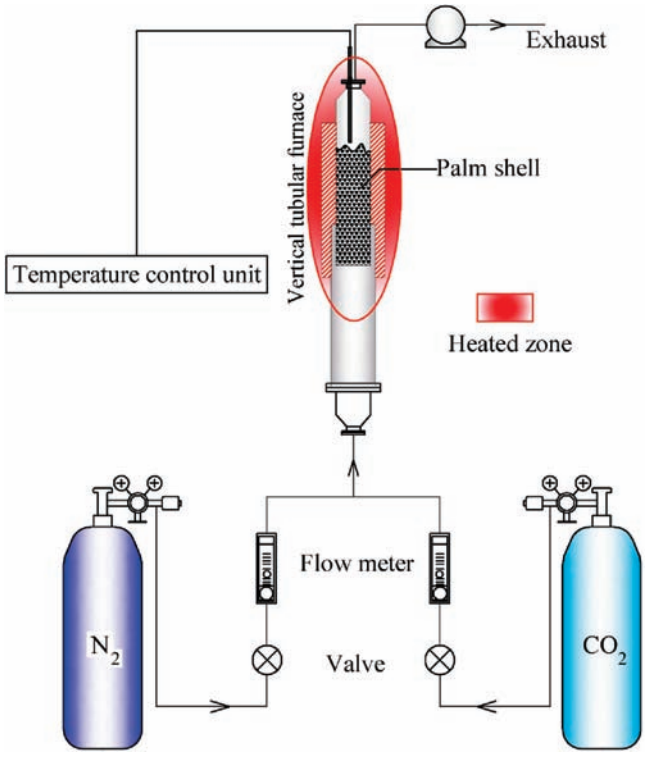

Figure 1. Schematic representation of the experimental setup for the preparation of activated carbon.

tion isotherms and kinetic models were used to interpret the experimental data.

Materials and Method

Adsorbent Raw Material. Palm shells were obtained from a local palm oil mill in Nibong Tebal, Malaysia. They were dried, crushed, and sieved to a particle size of (1 to 2) mm. The grounded palm shells were washed and oven-dried at 110 °C for 48 h.

Preparation of Activated Carbon. Palm shell like all lignocellulosic biomass comprises of three main natural polymers of cellulose (29 %), hemicellulose (17 %), and lignin (54 %).[27] Lignin is an aromatic polymer in the cell wall of woody biomass that cements the cellulosic fibers in plants.[21] The high lignin content of palm shell makes it hard, and a conventional physical or chemical activation process may not easily convert it to activated carbon. Therefore, in this study physiochemical activation was used as an effective technique, to prepare activated carbon from palm shell.

Figure 1 shows the schematic representation of the experimental setup. It consisted of a 310 stainless steel reactor (4 cm diameter and 40 cm length) equipped with a vertical tubular furnace. The batch experiments were conducted by loading 100 g of raw palm shell in the reactor. The carbonization process was performed under a N_2 flow of 500 mL·min^{-1}. The temperature of the reactor was increased at a rate of 15 °C·min^{-1} until it reached the carbonization temperature of 900 °C and was kept at this temperature for 1 h.[26,28] Selection of the carbonization temperature was based on the degradation profile of lignocellulosic biomass. Although the decomposition of hemicellulose followed by cellulose takes place in a narrow temperature range of (200 to 400) °C, the lignin decomposition process continues to 900 °C.[21] After carbonization, the samples were cooled down to room temperature under the N_2 flow. The carbonized samples were impregnated in NaOH (2 M) solution for 12 h. The NaOH solution was used as a chemical agent which causes the swelling of the carbonized shells. It also creates some porosity inside the chars and inhibits particle narrowing during the next heat treatment process.[21] The chemically activated shells were rinsed with distilled water until a neutral pH in the filtrate was achieved. Then, the samples were oven-dried at 110 °C for 3 h. In the next step, physical activation was carried out using CO_2 to develop the microporosity of the char and make it suitable for the adsorption process. This process was conducted while the chemically activated chars were reloaded in the reactor under a N_2 flow of 500 mL·min^{-1} until the temperature reached 900 °C. Then, the N_2 flow was stopped, and a CO_2 flow of 500 mL·min^{-1} was introduced into the column for 3 h. After that, the activated carbons were cooled to room temperature under N_2 flow. The so prepared activated carbons were kept in a desiccator for dye removal applications.

Characterization of the Activated Carbon. The activated carbon samples were characterized in terms of surface area and micropore volume by N_2 adsorption at 77 K in a Quantachrome Autosorb automated gas sorption system. The Brunauer−Emmett−Teller (BET) equation was used to measure the surface area. The micropore surface area was determined using the Dubinin−Radushkevich (DR) equation. To calculate the micropore volume and pore size distribution (PSD), density functional theory (DFT) was applied.[26,29] A Fourier transform infrared (FTIR) spectrum was recorded over the frequency range of (4000 to 400) cm^{-1} using a PerkinElmer FTIR 2000 spectrometer. Thermogravimetric analysis (TGA) was carried out using a TG analyzer model STDQ 600 at a heating rate of 10 °C·min^{-1} under a nitrogen flow of 10 mL·min^{-1}.

Adsorption Experiments. Batch sorption experiments were carried out using RB as adsorbate and palm shell derived activated carbon as adsorbent. RB was used as a coloring agent to prepare a stock dye solution of 2087.7 μmol·L^{-1} (1 g·L^{-1}). This solution was consequently diluted to prepare the required concentration of (41.8 to 208.8) μmol·L^{-1} [(20 to 100) mg·L^{-1}]. Dye removal experiments were conducted in a series of 250 mL Erlenmeyer flasks. A 100 mL aliquot of the dye solution was transferred to the flasks which contained 1 g of the activated carbon. The flasks were covered with parafilm and placed in a thermostatic shaker bath (Memmert, Germany) which was set at 100 rpm. Samples were taken at defined time intervals to determine the equilibrium concentration. The activated carbon was separated from the samples, and the supernatants were subjected to analysis. The absorbance of the samples was analyzed using a spectrophotometer (Thermospectronic, USA). A calibration curve was developed for a range of dye solutions with defined concentrations. Maximum absorbance was found to be at wavelength of 553 nm for RB. The residual dye concentration of the samples was determined using the calibration curve. The effect of various operational parameters of initial dye concentration, temperature, and pH on dye removal efficiency was examined. Dilute solutions of HCl (0.1 M) and NaOH (0.1 M) were used to adjust the pH to the desired values. In each set of experiments, the dye concentration of the samples was determined, and the dye removal efficiencies were calculated.

Results and Discussion

Characterization of the Activated Carbon. The textural characterization of the activated carbon was performed by N_2 adsorption, and the analysis result for the adsorption/desorption isotherms is depicted in Figure 2. The isotherm shows a type IV isotherm with a clear hysteresis loop, which is a typical characteristic of mesoporous materials. The hysteresis loop is observed wherever capillary evaporation in the mesopores occurs

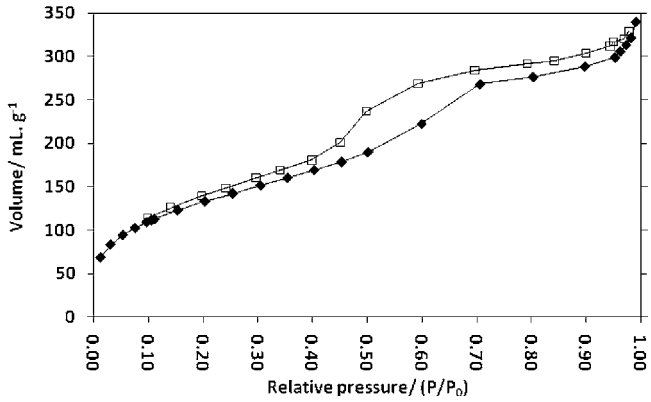

Figure 2. N_2 adsorption/desorption isotherms of the prepared activated carbon (N_2 900 °C/1 h, NaOH/12 h, CO_2 800 °C/3 h); ◆, adsorption and □, desorption.

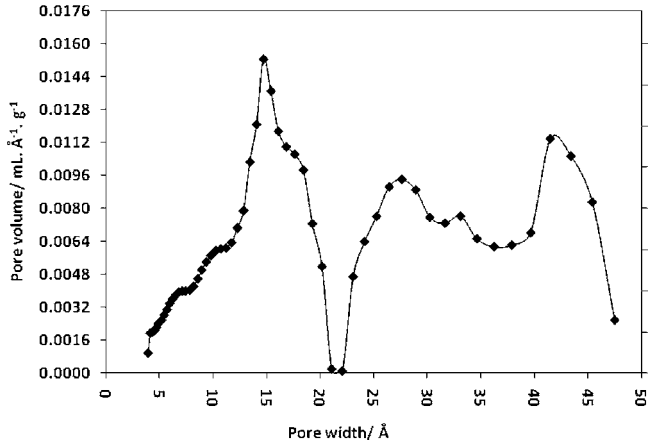

Figure 3. Pore size distribution of the prepared activated carbon (N_2 900 °C/1 h, NaOH/12 h, CO_2 800 °C/3 h).

Table 1. Textural Characteristics of the Palm Shell-Based Activated Carbon

parameter	obtained value
BET surface area, $S_{BET}/m^2 \cdot g^{-1}$	476.8
micropore surface area, $S_{DR}/m^2 \cdot g^{-1-1}$	569.8
total pore volume, $V_t/cm^3 \cdot g^{-1-1}$	0.460
micropore volume, $V_{mic}/cm^3 \cdot g^{-1}$	0.313
mesopore volume, $V_{mes}/cm^3 \cdot g^{-1}$	0.147

at a lower relative pressure than capillary condensation. The PSD which generally represents the structural homogeneity of activated carbon is shown in Figure 3. The PSD of the fabricated activated carbon confirms the presence of micropores (< 2 nm) and mesopores (< 50 nm)[30] in the activated carbon structure. The other textural properties of the prepared activated carbon are tabulated in Table 1.

Thermogravimetric Analysis (TGA). Figure 4 shows the thermogravimetric (TG) curves obtained for palm shell-based activated carbon under N_2. The typical TG curves of activated carbon consist of two stages corresponding to dehydration and active pyrolysis. The weight loss of activated carbon in the range of (50 to 100) °C can be confidently attributed to the release of adsorbed water, but the main weight loss started around 500 °C and continued to 900 °C. The weight loss in this range was probably due to the decomposition of stable surface oxygen groups such as carboxyl, ethers, and hydroxyls present in the structure of the activated carbon.[31]

FTIR Studies. Adsorption capacity is one of the important parameters in evaluating the performance of activated carbon. Adsorption capacity depends on the porosity of the activated

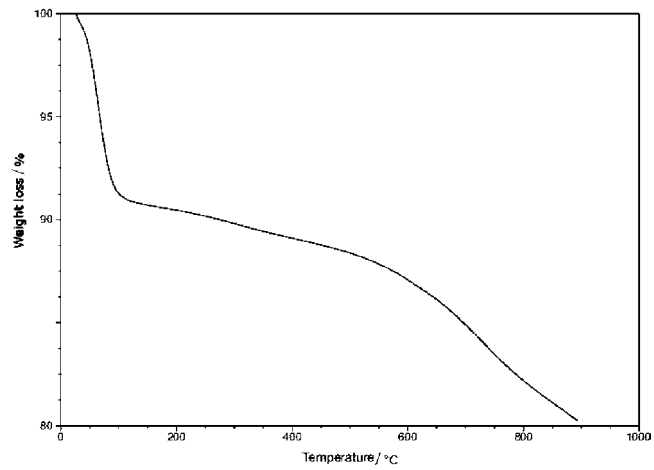

Figure 4. TGA of the fabricated activated carbon.

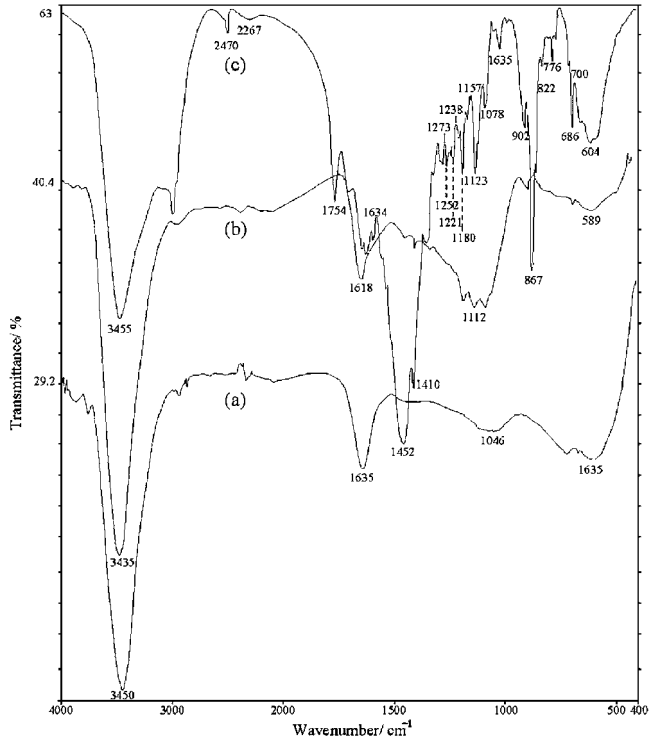

Figure 5. FTIR spectra of (a) pure activated carbon, (b) the intercalate of RB-activated carbon, and (c) RB.

carbon as well as the reactivity of its surface functional groups. Generally, carbonaceous materials contain surface complexes of heteroatoms such as oxygen, nitrogen, and hydrogen. The adsorptive properties of the adsorbent are significantly modified in the presence of such surface complexes. These heteroatoms create some degree of polarity on the carbon surface and thus improve the interaction of the carbon with polar materials. Oxygen surface groups which are mainly developed during the activation process are the most important surface groups that influence the surface properties and adsorptive behavior of the activated carbon.[32]

To obtain knowledge of the surface functional groups of the fabricated activated carbon, FTIR analysis was applied. Figure 5 shows the FTIR spectra of the pure activated carbon, RB, and the intercalate RB-activated carbon. The spectrum of pure activated carbon indicated the presence of an −OH stretching band at (3300 to 3500) cm^{-1} that from the literature is one of the most observed peaks in activated carbons.[33] The wide peak

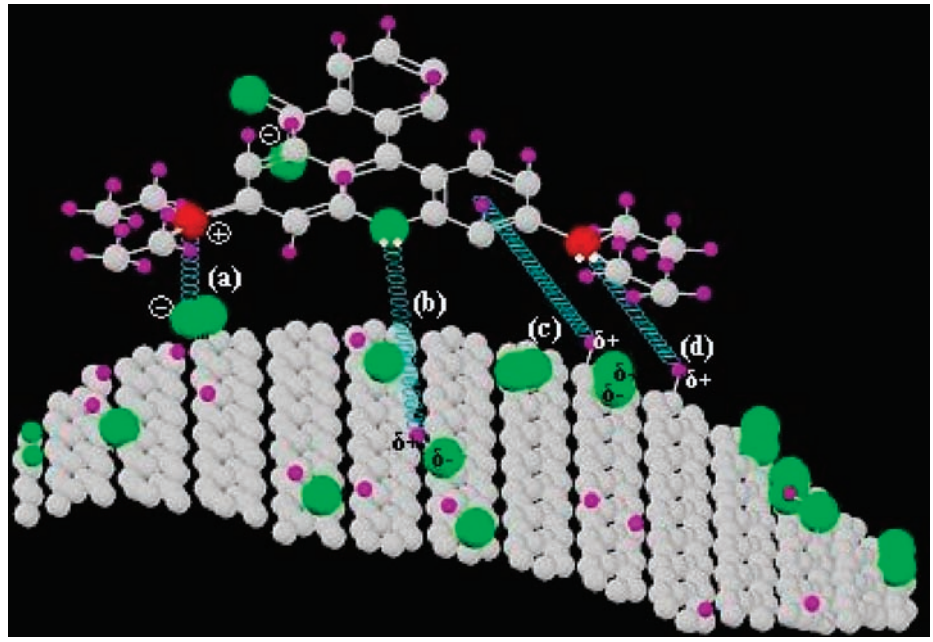

Figure 6. Schematic representation of RB adsorption on the activated carbon surface: green ●, oxygen; red ●, nitrogen; gray ●, carbon; purple ●, hydrogen. (a) Interaction between the carboxyl group of activated carbon and the electronegative groups in RB, (b) hydrogen bonding between the hydroxyl group of activated carbon and the oxygen of the xanthene ring, (c) hydrogen bonding between the hydroxyl group of the activated carbon and the aromatic ring in the RB molecule, and (d) electrostatic interaction between surface functional groups and dye molecules.

at (1540 to 1650) cm^{-1} shows the asymmetric stretch of the carboxylate ($-COO^-$) group,[34] and the broad peak at 1046 cm^{-1} represents the C−O−C functional group.[33] The small peaks located at (400 to 700) cm^{-1} could be the C−H out-of-plane bending in benzene derivatives that is quite common for activated carbon.[33] All of these surface functional groups of the activated carbon can interact with the dye molecules. Thus, the adsorption of RB on the activated carbon may be attributed to (i) chemical interaction between surface functional groups and dye molecules, (ii) electrostatic interaction between the RB molecules and electron-rich sites on the activated carbon surface, and (iii) weak physical forces, mainly hydrogen bonding and van der Waals interactions between the dye molecules and activated carbon.[35] Therefore, the adsorption of RB on the activated carbon may follow a complicated pattern which involves both physical and chemical adsorption. A similar complicated behavior of dye molecules on the adsorbent surface was also reported by Das et al.[35] who investigated the adsorption of RB on *Rhizopus oryzae* biomass. Figure 6 shows a schematic representation of some RB-activated carbon interactions that may be involved in the adsorption process. The adsorption of RB on the activated carbon surface may originate from the interaction between the carboxyl group of activated carbon and the electronegative groups in RB, hydrogen bonding between the hydroxyl group of activated carbon and the oxygen of the xanthene ring, hydrogen bonding between the hydroxyl group of the activated carbon and the aromatic ring in the RB molecule, and electrostatic interaction between surface functional groups and dye molecules.

Adsorption Isotherms. Adsorption isotherms are commonly used to evaluate the performance of adsorbents in adsorption processes. They describe the interaction between adsorbate and adsorbent and also represent the surface properties of the adsorbent.[36] In this study, various adsorption isotherms (Langmuir, Freundlich, and Temkin) were used to interpret the obtained experimental data.

The Langmuir isotherm which represents monolayer coverage of the adsorbate on the adsorbent surface is expressed as follows:[37]

$$\frac{C_e}{q_e} = \frac{1}{K_L q_{max}} + \frac{C_e}{q_{max}} \quad (1)$$

where C_e is the equilibrium concentration of RB in the aqueous phase ($mol \cdot L^{-1}$), K_L is the Langmuir adsorption constant ($L \cdot mol^{-1}$), q_{max} is the maximum adsorption capacity of the adsorbent ($mol \cdot g^{-1}$), and q_e is the amount of RB adsorbed per mass of adsorbent at equilibrium ($mol \cdot g^{-1}$). The Freundlich isotherm indicates surface heterogeneity of the adsorbent as well as multilayer coverage on the surface. The linearized form of this isotherm is given as:[38]

$$\log q_e = \log K_F + \frac{1}{n} \log C_e \quad (2)$$

where n shows the adsorption intensity in the Freundlich equation and K_F is the Freundlich adsorption capacity [$(mol \cdot g^{-1}) \cdot (L \cdot g^{-1})^{1/n}$]. To study the heat of adsorption and adsorbate−adsorbent interaction on the adsorbent surface, the Temkin isotherm is applied. Equation 3 shows the linearized form of this isotherm:[25]

$$q_e = B_1 \ln K_T + B_1 \ln C_e \quad (3)$$

where B_1 is the Temkin adsorption constant and K_T is the equilibrium binding constant ($L \cdot mol^{-1}$).

Table 2 tabulates the obtained isotherm constants and coefficients which were calculated from the slope and intercept of the linearized models. Among the implemented adsorption isotherms, the best fit was obtained with the Langmuir isotherm with a regression coefficient, R^2 of 0.9751. The experimental

Table 2. Constants and Coefficients of Various Applied Isotherms

adsorption isotherm	parameter	obtained value
Langmuir	q_{max}/mol·g^{-1}	$2.92 \cdot 10^{-6}$
	K_L/L·mol^{-1}	$-5.13 \cdot 10^{4}$
	R^2	0.9751
Freundlich	K_F/ [(mol·g^{-1})·(L·g^{-1})$^{1/n}$]	$1.64 \cdot 10^{-7}$
	n	3.82
	R^2	0.8659
Temkin	B_1	$-5 \cdot 10^{-7}$
	K_T/L·mol^{-1}	403.43
	R^2	0.9116

data were fairly well fitted by the Temkin isotherm (R^2 = 0.9116) but did not show good agreement with the Freundlich model (R^2 = 0.8659).

Figure 7 shows the linearized Temkin adsorption isotherm applied to the experimental data. It is a plot of q_e versus ln C_e where coefficients B_1 and K_T are easily obtained from the slope and intercept of the linearized isotherm. On the basis of the Temkin adsorption isotherm, the heat of adsorption linearly decreases as the thickness of the dye layer on the adsorbent gradually increases, which results from reduced adsorbate−adsorbent interaction. This model also assumes uniform distribution of binding sites on the surface of the adsorbent.[39] The linear plot of this isotherm shows a negative slope which implies the existence of a repulsive lateral interaction in the adsorption layer.[40,41] At first the dye molecules occupy the active sites on the carbon surface. As the dye coverage of the surface increases, the repulsive lateral interaction between the neighboring dye molecules reduces the adsorption capacity. In fact, the bond weakening which arises from the repulsive lateral interaction of the RB_{ads}−RB_{ads} reduces the RB-activated carbon surface bond energy and causes the desorption of dye molecules from the adsorption layer.

The linearized form of the Langmuir equation is depicted in Figure 8 which is a plot of C_e/q_e versus C_e. This plot has led to a straight line with the slope of $1/q_{max}$ and intercept of $1/K_L \cdot q_{max}$. To assess the Langmuir isotherm, a dimensionless equilibrium parameter R_L is used. This parameter (R_L) is expressed by the following equation:[42]

$$R_L = \frac{1}{(1 + K_L C_0)} \tag{4}$$

where K_L is the Langmuir constant and C_o is the initial dye concentration. The value of $R_L > 1$ represents an unfavorable, $R_L = 1$ linear, $0 < R_L < 1$ favorable, and $R_L = 0$ irreversible adsorption process. In this study, R_L values of 0.3179, 0.2374, 0.1892, 0.1348, 0.1045, and 0.0853 were obtained for initial dye concentrations of (41.8, 62.6, 83.5, 125.3, 167.1, and 208.8) μmol·L^{-1}, respectively, which indicates favorable adsorption for all dye concentrations. The obtained experimental data were fairly well-described by the Langmuir isotherm which represents monolayer adsorption of the dye molecules on the adsorbent.[25,36,43] Monolayer adsorption was also confirmed by the deviation of the experimental data from the Freundlich isotherm (see Figure 9), which shows multilayer coverage of the adsorbent. The Langmuir isotherm also represents a homogeneous surface of the fabricated activated carbon in terms of functional groups and bonding energy.[36] A uniform distribution of binding sites on the fabricated adsorbent surface was also confirmed by the Temkin isotherm.

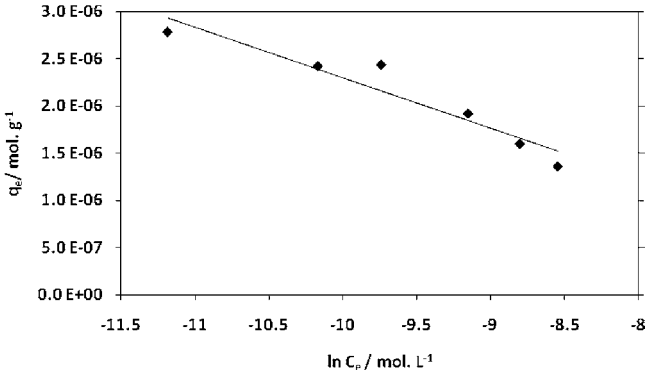

Figure 7. Temkin isotherm for RB adsorption on activated carbon (C_0 = (41.8 to 208.8) μmol·L^{-1}; T = 30 °C; pH = 4.5).

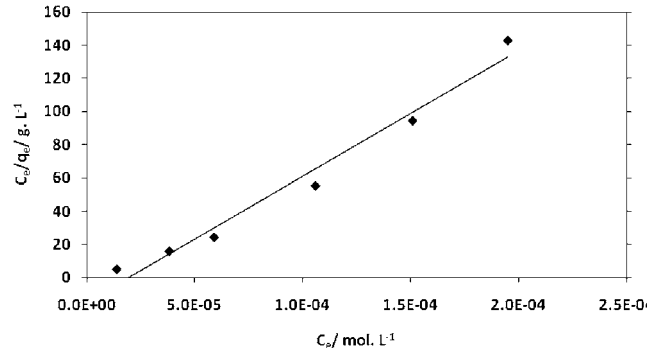

Figure 8. Langmuir isotherm for RB adsorption on activated carbon (C_0 = (41.8 to 208.8) μmol·L^{-1}; T = 30 °C; pH = 4.5).

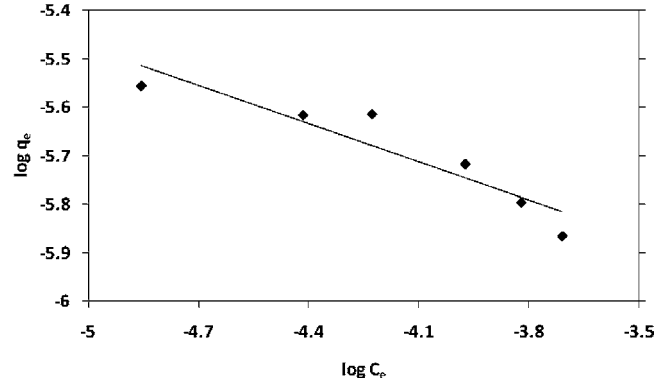

Figure 9. Freundlich isotherm for RB adsorption on activated carbon (C_0 = (41.8 to 208.8) μmol·L^{-1}; T = 30 °C; pH = 4.5).

Kinetic Studies. Kinetic models have been proposed to determine the mechanism of the adsorption process which provides useful data to improve the efficiency of the adsorption and feasibility of process scale-up.[43] Physical and chemical properties of the adsorbents as well as mass transfer processes are some influential parameters to determine the adsorption mechanism. In the present investigation, the mechanism of the adsorption process was studied by fitting pseudofirst- and second-order reactions to the experimental data. The Lagergren pseudofirst-order model is given by the following equation:[44]

$$\ln(q_e - q_t) = \ln(q_e) - k_1 t \tag{5}$$

where q_e and q_t are the sorption capacities at equilibrium and time t, respectively (mol·g^{-1}), and k_1 represents the rate constant of the pseudofirst-order kinetic model (min^{-1}). The data obtained for sorption of RB on activated carbon based on the pseudofirst-order kinetic model showed that the adsorption kinetics were not in a good agreement with the pseudofirst-order model. The

Table 3. Kinetic Parameters and Coefficients of the Pseudosecond-Order Reaction

		pseudosecond-order equation			
parameter	values	q_e(exp.)/mol·g^{-1}	q_e(cal.)/mol·g^{-1}	k_2/g·mol^{-1}·h^{-1}	R^2
concentration/μmol·L^{-1}	41.8	$2.78358 \cdot 10^{-6}$	$2.86322 \cdot 10^{-6}$	$7.44042 \cdot 10^{5}$	0.9912
	62.6	$2.44171 \cdot 10^{-6}$	$2.65835 \cdot 10^{-6}$	$5.43759 \cdot 10^{5}$	0.9831
	83.5	$2.43563 \cdot 10^{-6}$	$2.55262 \cdot 10^{-6}$	$5.10353 \cdot 10^{5}$	0.9868
	125.3	$1.92067 \cdot 10^{-6}$	$2.41467 \cdot 10^{-6}$	$3.04621 \cdot 10^{5}$	0.9741
	167.1	$1.60056 \cdot 10^{-6}$	$2.26452 \cdot 10^{-6}$	$2.00607 \cdot 10^{5}$	0.9354
	208.8	$1.36395 \cdot 10^{-6}$	$1.61956 \cdot 10^{-6}$	$1.48126 \cdot 10^{5}$	0.9895
pH	3	$5.9700 \cdot 10^{-6}$	$6.3496 \cdot 10^{-6}$	$8.3553 \cdot 10^{5}$	0.9999
	5	$2.90884 \cdot 10^{-6}$	$3.1183 \cdot 10^{-6}$	$6.4445 \cdot 10^{5}$	0.9974
	7	$2.78358 \cdot 10^{-6}$	$3.1118 \cdot 10^{-6}$	$4.2911 \cdot 10^{5}$	0.9968
	11	$2.76966 \cdot 10^{-6}$	$2.9432 \cdot 10^{-6}$	$4.2681 \cdot 10^{5}$	0.9999
temperature/°C	30	$2.42171 \cdot 10^{-6}$	$2.55835 \cdot 10^{-6}$	$5.13759 \cdot 10^{5}$	0.9831
	40	$2.56089 \cdot 10^{-6}$	$2.7231 \cdot 10^{-6}$	$6.6898 \cdot 10^{5}$	0.9956
	50	$2.65832 \cdot 10^{-6}$	$2.7791 \cdot 10^{-6}$	$8.5687 \cdot 10^{5}$	0.9986

inapplicability of the Lagergren model to describe the kinetics of RB adsorption was also reported by Lata et al.[38] who investigated the adsorption of this dye on chemically activated *Parthenium* biomass.

The linearized form of the pseudosecond-order kinetic model is represented as follows:[44]

$$\frac{t}{q_t} = \frac{1}{k_2 q_e^{\,2}} + \frac{t}{q_e} \tag{6}$$

where q_e and q_t are the sorption capacities at equilibrium and time t, respectively (mol·g^{-1}), and k_2 is the equilibrium rate constant of the pseudosecond-order adsorption (g·mol^{-1}·h^{-1}). Table 3 summarizes the parameters and coefficients of the pseudosecond-order kinetic model applied to the experimental data. Results show that the values of R^2 were close to unity for most cases, and the calculated values of q_e were in agreement with the experimental data. As the pH of the solution increased from 3 to 11, the sorption coefficient decreased from (8.35 to 4.26)·10^5 g·mol^{-1}·h^{-1}, and the adsorption capacity also decreased from (6.35 to 2.94) μmol·g^{-1}, which confirmed the validity of the obtained experimental results. Increasing the temperature from (30 to 50) °C improved the adsorption capacity, and sorption coefficients as such trends were expected from previous experiments. The variations of theoretical q_e with concentration were also in the same trend as the experimental ones. The values of the sorption coefficient also decreased from (7.44 to 1.48)·10^5 g·mol^{-1}·h^{-1}, as the initial RB concentration was increased from (41.8 to 208.8) μmol·L^{-1}. Such agreement between the obtained experimental data and calculated parameters implies that the adsorption of RB on activated carbon follows a pseudosecond-order kinetic model.

Thermodynamic Studies. The thermodynamic parameters of ΔG, ΔH, and ΔS for the adsorption of RB on activated carbon were calculated based on the following equations:

$$\Delta G = -RT \ln K_C \tag{7}$$

where R is the gas constant, T is the absolute temperature, and K_C is the equilibrium constant which is obtained from the following equation:

$$K_C = \frac{C_A}{C_S} \tag{8}$$

where C_A and C_S are the equilibrium concentration of dye on the adsorbent and in the solution. The standard enthalpy and entropy of the adsorption process can be calculated from the van't Hoff equation:[25]

$$\ln K_C = \frac{-\Delta H}{RT} + \frac{\Delta S}{R} \tag{9}$$

The values of ΔH and ΔS are easily obtained from the linear plot of ln K_C versus $1/T$. The linearized form of the van't Hoff equation is depicted in Figure 10. A positive value of enthalpy change ($\Delta H = 6200$ J·mol^{-1}) indicates the endothermic nature of the adsorption process. In endothermic processes where the reaction is not favored energetically, a favorable change in entropy may provide the necessary driving force. Thus, the positive value of entropy change ($\Delta S = 17.2$ J·mol^{-1}·K^{-1}) shows the affinity of the fabricated adsorbent toward RB molecules. The ΔG values of (−1161, −963, and −821) J·mol^{-1} were obtained for temperatures of (30, 40, and 50) °C, respectively. The negative value of ΔG implies that the adsorption process leads to a decrease in Gibbs energy and confirms the spontaneous nature of the adsorption process.[45]

Although a positive value was obtained for the enthalpy and entropy changes in the adsorption process, their small values indicate the existence of an electrostatic repulsive force.[31] In this case, there exists a repulsive force between the charged carbon surfaces and the RB ions which have the same charge as the carbon surface. Such electrostatic repulsion causes the weakening of the adsorption forces and increases the degree of freedom of the RB molecules on the carbon surface. To overcome such repulsive forces, the system must take some energy from the environment to adsorb the RB ions on the

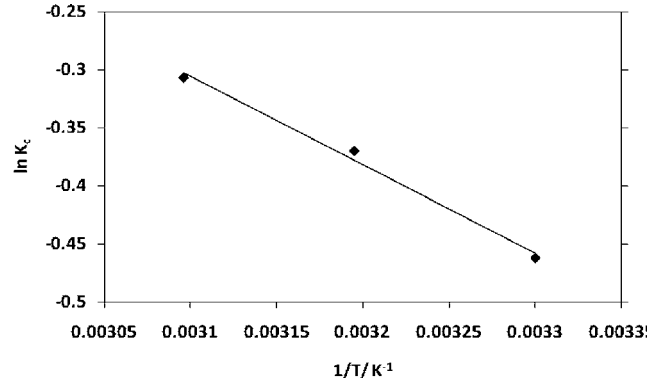

Figure 10. van't Hoff equation for RB adsorption.

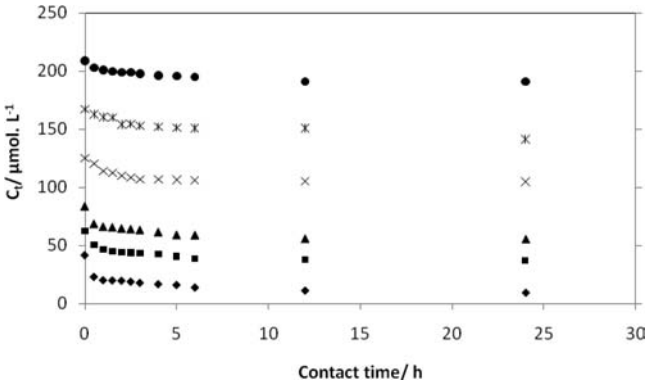

Figure 11. Variation of RB concentration with respect to time at pH = 4.5 and T = 30 °C. ◆, C_0 = 41.8 μmol·L^{-1}; ■, C_0 = 62.6 μmol·L^{-1}; ▲, C_0 = 83.5 μmol·L^{-1}; ×, C_0 = 125.3 μmol·L^{-1}; ∗, C_0 = 167.1 μmol·L^{-1}; ●, C_0 = 208.8 μmol·L^{-1}.

activated carbon surface. Although such adsorption processes are endothermic in nature, the electrostatic repulsion, which acts against the adsorption force, leads to an endothermic process with small values of enthalpy and entropy changes.

Effect of Initial Dye Concentration. Batch adsorption of RB from aqueous solution was carried out, while the initial dye concentration was varied in the range of (41.8 to 208.8) μmol·L^{-1}. The variation of dye concentration with respect to time is depicted in Figure 11. The obtained results revealed that, after a contact time of 6 h, the amount of dye adsorbed on the activated carbon did not change significantly. Therefore, this time was considered as the equilibrium time in the rest of the adsorption experiments. The equilibrium concentrations of (13.6, 39.2, 59.1, 105.1, 151.1, and 195.1) μmol·L^{-1} were achieved at 6 h for initial dye concentrations of (41.8, 62.6, 83.5, 125.3, 167.1, and 208.8) μmol·L^{-1}, respectively. It was found that the dye removal efficiency of the fabricated adsorbent was not considerable at a solution temperature of 30 °C and pH of 4.5. This may originate from (i) the repulsive lateral interaction of the RB_{ads}−RB_{ads} molecules in the adsorption layer whose existence was confirmed by the negative slope of the Temkin isotherm, (ii) an electrostatic repulsive force between the carbon surface and the RB ions due to the charge similarity which was discussed above, and (iii) the microporus structure of the fabricated activated carbon. It is important to note that micropores are often the major contribution to the adsorption capacity but the adsorbate molecule should be small enough to penetrate into the micropores. For example, the molecular diameter of methylene blue is around 0.8 nm, but the minimum diameter of micropores that allow methylene blue to enter is estimated to be around 1.3 nm.[31] Thus, the average pore diameter of the adsorbent should be approximately 2 to 3 times that of the adsorbate for easy diffusion into the pores. The molecular size of RB is around 1.8 nm,[25] and the micropore diameter is less than 2 nm. Therefore, most micropores were unavailable to the RB molecules, and RB is likely adsorbed in mesopores. Because of the large proportion of micropores (69 %) in comparison to mesopores (31 %) in the fabricated activated carbon, a considerable adsorption capacity was not achievable in the experiments.

Effect of Temperature. Figure 12 shows the effect of solution temperature on adsorption capacity at various temperatures of (30, 40, and 50) °C at a constant RB concentration of 62.6 μmol·L^{-1}. As illustrated in this figure, the amount of RB adsorbed per mass of activated carbon increased as the temperature was raised from (30 to 50) °C. The endothermic nature of the adsorption process justifies the temperature dependence

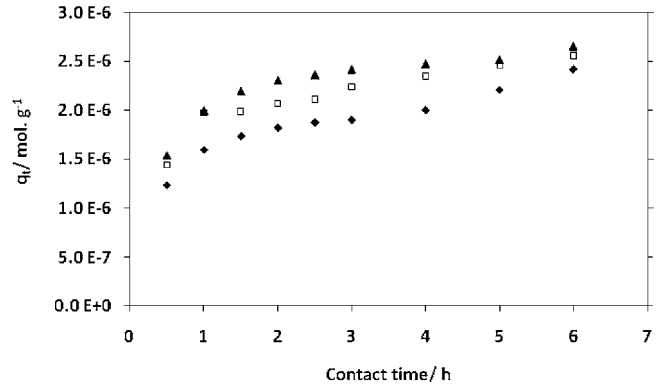

Figure 12. Effect of temperature on adsorption capacity at C_0 = 62.6 μmol·L^{-1} and pH = 4.5. ◆, T = 30 °C; □, T = 40 °C; ▲, T = 50 °C.

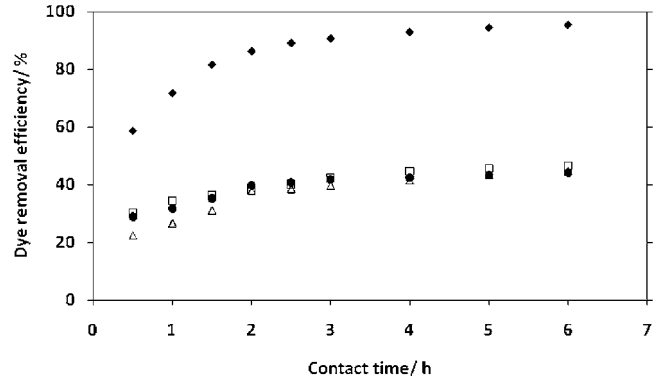

Figure 13. Effect of pH on RB removal efficiency at C_0 = 62.6 μmol·L^{-1} and T = 50 °C. ◆, pH = 3; □, pH = 5; △, pH = 7; ●, pH = 11.

of such a process. As explained earlier, an electrostatic repulsive force is in contrast with the adsorption force on the activated carbon surface. The system requires some energy from the environment to overcome such repulsive forces and adsorb the RB molecules on the carbon surface. At high temperatures, more energy is provided for the system which is likely to facilitate the attachment of RB on the carbon surface. As a result, the adsorption capacity of the adsorbent improves at high temperature. A similar trend was observed by Gad and El-Sayed[25] who investigated the adsorption of RB on bagasse pith derived activated carbon in the range of (20 to 70) °C. Guo et al.[46] also studied the effect of temperature on RB adsorption on a rice husk-based activated carbon. In their experiments, the solution temperature was increased from (30 to 80) °C, and it was observed that the adsorption capacity was significantly improved. They concluded that the average pore size of the carbon (2 nm) was close to the molecular size of RB (1.8 nm). Thus, adsorption of the RB molecule at the pore entrance would have caused a hindrance for the subsequent entrance of dye molecules. As the temperature increased, the intraparticle diffusion rate of the dye into the porous structure of carbon which is an endothermic process was improved. As a result, the adsorption capacity increased along with solution temperature.

Effect of Dye Solution pH. To investigate the effect of solution pH on dye removal efficiency, the pH of the solution was varied from 3 to 11, while the dye concentration was kept constant at 62.6 μmol·L^{-1}. The obtained results are presented in Figure 13. The achieved results showed that, as the pH was increased from 3 to 11, the dye removal efficiency drastically decreased from (95 to 40) % after a contact time of 6 h. It is well-known that adsorption characteristics of the adsorbents are significantly influenced by the pH of the solution.[43] In fact, the amount of dye adsorbed on the surface of the adsorbent is

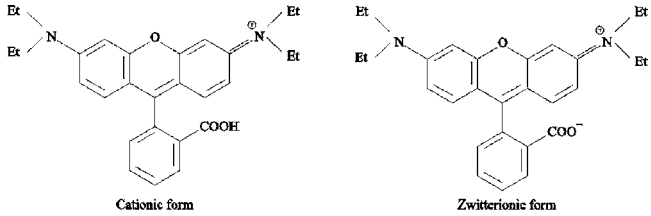

Figure 14. Molecular forms of RB.

influenced by the surface charge and consequently solution pH. RB exists in two forms (cationic and zwitterionic) in polar solvents as depicted in Figure 14. The transformation of the cationic to zwitterionic form occurs at pH values of greater than 3.7 (pK_a of RB) by deprotonation of the carboxyl group of the cationic (RB^+) form.[16] Electrostatic interactions between the xanthene and the carboxyl group of RB monomers causes the aggregation of RB to form dimers and hinders the adsorption of dye molecules into the pores.[25,43] As a result, the amount of dye adsorbed on the activated carbon decreased with an increase in pH of the solution. Guo et al.[46] studied the effect of pH on RB adsorption using rice husk-based carbon and reported a pH of 3.45 as the optimum pH at which maximum dye removal was achieved.

Conclusion

Palm shell was utilized as a potential lignocellolusic waste material to prepare activated carbon by physiochemical activation. The palm shell-based activated carbon was successfully used in batch experiments to remove RB from aqueous solution. The obtained results confirmed the dye removal ability of the prepared activated carbon, as a maximum removal efficiency of 95 % was achieved under appropriate conditions. The equilibrium data were analyzed using various adsorption isotherms. The achieved experimental data were fairly well-represented by the Langmuir and Temkin adsorption isotherms. Also, the best fit was obtained with a pseudosecond-order kinetic model while investigating the adsorption kinetics.

Literature Cited

(1) Shakir, K.; Elkafrawy, A.; Ghoneimy, H.; Elrab Beheir, S.; Refaat, M. Removal of rhodamine B (a basic dye) and thoron (an acidic dye) from dilute aqueous solutions and wastewater simulants by ion flotation. *Water Res.* **2010**, *44*, 1449–1461.

(2) Sachdeva, S.; Kumar, A. Preparation of nanoporous composite carbon membrane for separation of rhodamine B dye. *J. Membr. Sci.* **2009**, *329*, 2–10.

(3) Mehrdad, A.; Hashemzadeh, R. Ultrasonic degradation of Rhodamine B in the presence of hydrogen peroxide and some metal oxide. *Ultrason. Sonochem.* **2010**, *17*, 168–172.

(4) Muthuraman, G.; Teng, T. Extraction and recovery of rhodamine B, methyl violet and methylene blue from industrial wastewater using D2EHPA as an extractant. *J. Ind. Eng. Chem.* **2009**, *15*, 841–846.

(5) Yuan, Q.; Liu, Y.; Li, L.; Li, Z.; Fang, C.; Duan, W.; Li, X.; Yan, C. Highly ordered mesoporous titania-zirconia photocatalyst for applications in degradation of rhodamine-B and hydrogen evolution. *Microporous Mesoporous Mater.* **2009**, *124*, 169–178.

(6) Li, Y.; Sun, S.; Ma, M.; Ouyang, Y.; Yan, W. Kinetic study and model of the photocatalytic degradation of rhodamine B (RhB) by a TiO_2-coated activated carbon catalyst: Effects of initial RhB content, light intensity and TiO_2 content in the catalyst. *Chem. Eng. J.* **2008**, *142*, 147–155.

(7) He, Z.; Yang, S.; Ju, Y.; Sun, C. Microwave photocatalytic degradation of Rhodamine B using TiO_2 supported on activated carbon: Mechanism implication. *J. Environ. Sci.* **2009**, *21*, 268–272.

(8) Song, X.; Wu, J.; Yan, M. Photocatalytic and photoelectrocatalytic degradation of aqueous Rhodamine B by low-temperature deposited anatase thin films. *Mater. Chem. Phys.* **2008**, *112*, 510–515.

(9) Belver, C.; Adán, C.; Fernández-García, M. Photocatalytic behaviour of Bi_2MO_6 polymetalates for rhodamine B degradation. *Catal. Today* **2009**, *143*, 274–281.

(10) Xiao, Y.; Dang, L.; An, L.; Bai, S.; Lei, Z. Photocatalytic Degradation of Rhodamine B and Phenol by TiO_2 Loaded on Mesoporous Graphitic Carbon. *Chin. J. Catal.* **2008**, *29*, 31–36.

(11) He, Z.; Sun, C.; Yang, S.; Ding, Y.; He, H.; Wang, Z. Photocatalytic degradation of rhodamine B by Bi_2WO_6 with electron accepting agent under microwave irradiation: Mechanism and pathway. *J. Hazard. Mater.* **2009**, *162*, 1477–1486.

(12) Martínez-de la Cruz, A.; Pérez, U. Photocatalytic properties of $BiVO_4$ prepared by the co-precipitation method: Degradation of rhodamine B and possible reaction mechanisms under visible irradiation. *Mater. Res. Bull.* **2010**, *45*, 135–141.

(13) Behnajady, M.; Modirshahla, N.; Tabrizi, S.; Molanee, S. Ultrasonic degradation of Rhodamine B in aqueous solution: Influence of operational parameters. *J. Hazard. Mater.* **2008**, *152*, 381–386.

(14) Merouani, S.; Hamdaoui, O.; Saoudi, F.; Chiha, M.; Pétrier, C. Influence of bicarbonate and carbonate ions on sonochemical degradation of Rhodamine B in aqueous phase. *J. Hazard. Mater.* **2010**, *175*, 593–599.

(15) Ruot, B.; Plassais, A.; Olive, F.; Guillot, L.; Bonafous, L. TiO_2-containing cement pastes and mortars: Measurements of the photocatalytic efficiency using a rhodamine B-based colourimetric test. *Sol. Energy* **2009**, *83*, 1794–1801.

(16) Yu, J.; Li, B.; Sun, X.; Jun, Y.; Chi, R. Adsorption of methylene blue and rhodamine B on baker's yeast and photocatalytic regeneration of the biosorbent. *Biochem. Eng. J.* **2009**, *45*, 145–151.

(17) Das, S.; Ghosh, P.; Ghosh, I.; Guha, A. Adsorption of rhodamine B on Rhizopus oryzae: Role of functional groups and cell wall components. *Colloids Surf., B* **2008**, *65*, 30–34.

(18) Ju, D.; Byun, I.; Park, J.; Lee, C.; Ahn, G.; Park, T. Biosorption of a reactive dye (Rhodamine-B) from an aqueous solution using dried biomass of activated sludge. *Bioresour. Technol.* **2008**, *99*, 7971–7975.

(19) Hii, S.; Yong, S.; Wong, C. Removal of rhodamine B from aqueous solution by sorption on Turbinaria conoides (Phaeophyta). *J. Appl. Phycol.* **2009**, *21*, 625–631.

(20) Muthuraman, G.; Teng, T. Use of vegetable oil in supported liquid membrane for the transport of Rhodamine B. *Desalination* **2009**, *249*, 1062–1066.

(21) Mohamed, A. R.; Mohammadi, M.; Darzi, G. N. Preparation of carbon molecular sieve from lignocellulosic biomass: A review. *Renewable Sustainable Energy Rev.* **2010**, *14*, 1591–1599.

(22) Parab, H.; Sudersanan, M.; Shenoy, N.; Pathare, T.; Vaze, B. Use of Agro-Industrial Wastes for Removal of Basic Dyes from Aqueous Solutions. *Clean: Soil, Air, Water* **2009**, *37*, 963–969.

(23) Panda, G.; Das, S.; Guha, A. Jute stick powder as a potential biomass for the removal of congo red and rhodamine B from their aqueous solution. *J. Hazard. Mater.* **2009**, *164*, 374–379.

(24) Sureshkumar, M.; Namasivayam, C. Adsorption behavior of Direct Red 12B and Rhodamine B from water onto surfactant-modified coconut coir pith. *Colloids Surf., A* **2008**, *317*, 277–283.

(25) Gad, H. M. H.; El-Sayed, A. A. Activated carbon from agricultural by-products for the removal of Rhodamine-B from aqueous solution. *J. Hazard. Mater.* **2009**, *168*, 1070–1081.

(26) Ahmad, M.; Wan Daud, W.; Aroua, M. Adsorption kinetics of various gases in carbon molecular sieves (CMS) produced from palm shell. *Colloids Surf., A* **2008**, *312*, 131–135.

(27) Adinata, D.; Wan Daud, W.; Aroua, M. Production of carbon molecular sieves from palm shell based activated carbon by pore sizes modification with benzene for methane selective separation. *Fuel Process. Technol.* **2007**, *88*, 599–605.

(28) Daud, W.; Ahmad, M.; Aroua, M. Carbon molecular sieves from palm shell: Effect of the benzene deposition times on gas separation properties. *Sep. Purif. Technol.* **2007**, *57*, 289–293.

(29) Zhang, T.; Walawender, W.; Fan, L. Preparation of carbon molecular sieves by carbon deposition from methane. *Bioresour. Technol.* **2005**, *96*, 1929–1935.

(30) Daud, W.; Ali, W. Comparison on pore development of activated carbon produced from palm shell and coconut shell. *Bioresour. Technol.* **2004**, *93*, 63–69.

(31) Rodriguez, A.; Garcia, J.; Ovejero, G.; Mestanza, M. Adsorption of anionic and cationic dyes on activated carbon from aqueous solutions: Equilibrium and kinetics. *J. Hazard. Mater.* **2009**, *172*, 1311–1320.

(32) Rodriguez-Reinoso, F.; Sepul-veda-Escribano, A.; Nalwa, H. S. *Handbook of surfaces and interfaces of materials*; Academic Press: San Diego, 2001.

(33) Sumathi, S.; Bhatia, S.; Lee, K.; Mohamed, A. Selection of best impregnated palm shell activated carbon (PSAC) for simultaneous removal of SO_2 and NO_x. *J. Hazard. Mater.* **2010**, *176*, 1093–1096.

(34) Smith, B. *Infrared spectral interpretation: a systematic approach*; CRC: London, 1999.

(35) Das, S.; Bhowal, J.; Das, A.; Guha, A. Adsorption behavior of rhodamine B on Rhizopus oryzae biomass. *Langmuir* **2006**, *22*, 7265–7272.

(36) Ofomaja, A. Equilibrium studies of copper ion adsorption onto palm kernel fibre. *J. Environ. Manage.* **2010**, *91* (7), 1491−1499.
(37) Sharma, Y.; Sinha, A.; Upadhyay, S. Characterization and Adsorption Studies of Cocos nucifera L. Activated Carbon for the Removal of Methylene Blue from Aqueous Solutions. *J. Chem. Eng. Data* **2010**, *55*, 2662–2667.
(38) Lata, H.; Garg, V.; Gupta, R. Adsorptive removal of basic dye by chemically activated Parthenium biomass: equilibrium and kinetic modeling. *Desalination* **2008**, *219*, 250–261.
(39) Sharma, Y.; Upadhyay, S. Removal of a Cationic Dye from Wastewaters by Adsorption on Activated Carbon Developed from Coconut Coir. *Energy Fuels* **2009**, *23*, 2983–2988.
(40) De Souza, F.; Spinelli, A. Caffeic acid as a green corrosion inhibitor for mild steel. *Corros. Sci.* **2009**, *51*, 642–649.
(41) Khaled, K. Monte Carlo simulations of corrosion inhibition of mild steel in 0.5 M sulphuric acid by some green corrosion inhibitors. *J. Solid State Electrochem.* **2009**, *13*, 1743–1756.
(42) Sharma, Y. Optimization of Parameters for Adsorption of Methylene Blue on a Low-Cost Activated Carbon. *J. Chem. Eng. Data* **2009**, *55*, 435–439.
(43) Eftekhari, S.; Habibi-Yangjeh, A.; Sohrabnezhad, S. Application of AlMCM-41 for competitive adsorption of methylene blue and rhodamine B: Thermodynamic and kinetic studies. *J. Hazard. Mater.* **2010**, *178*, 349–355.
(44) Sun, D.; Zhang, X.; Wu, Y.; Liu, X. Adsorption of anionic dyes from aqueous solution on fly ash. *J. Hazard. Mater.* **2010**, *181*, 335–342.
(45) Sharma, Y. Thermodynamics of removal of cadmium by adsorption on an indigenous clay. *Chem. Eng. J.* **2008**, *145*, 64–68.
(46) Guo, Y.; Zhao, J.; Zhang, H.; Yang, S.; Qi, J.; Wang, Z.; Xu, H. Use of rice husk-based porous carbon for adsorption of Rhodamine B from aqueous solutions. *Dyes Pigm.* **2005**, *66*, 123–128.

Received for review July 10, 2010. Accepted October 23, 2010. The authors gratefully acknowledge the Universiti Sains Malaysia and the Ministry of Science, Technology and Innovation Malaysia for funding this project in the form of a USM Research University Grant (1001/PJKIMIA/814004) and a Science Fund Grant (305/PJKIMIA/6013327), respectively.

JE100730A